Magnetic Fields at Uranus

NORMAN F. NESS, MARIO H. ACUÑA, KENNETH W. BEHANNON, LEONARD F. BURLAGA, JOHN E. P. CONNERNEY, RONALD P. LEPPING, FRITZ M. NEUBAUER

The magnetic field experiment on the Voyager 2 spacecraft revealed a strong planetary magnetic field of Uranus and an associated magnetosphere and fully developed bipolar magnetic tail. The detached bow shock wave in the solar wind supersonic flow was observed upstream at 23.7 Uranus radii (1 R_U = 25,600 km) and the magnetopause boundary at 18.0 R_U, near the planet-sun line. A maximum magnetic field of 413 nanotesla was observed at 4.19 R_U, just before closest approach. Initial analyses reveal that the planetary magnetic field is well represented by that of a dipole offset from the center of the planet by 0.3 R_U. The angle between Uranus' angular momentum vector and the dipole moment vector has the surprisingly large value of 60 degrees. Thus, in an astrophysical context, the field of Uranus may be described as that of an oblique rotator. The dipole moment of 0.23 gauss R_U^3, combined with the large spatial offset, leads to minimum and maximum magnetic fields on the surface of the planet of approximately 0.1 and 1.1 gauss, respectively. The rotation period of the magnetic field and hence that of the interior of the planet is estimated to be 17.29 ± 0.10 hours; the magnetotail rotates about the planet-sun line with the same period. The large offset and tilt lead to auroral zones far from the planetary rotation axis poles. The rings and the moons are embedded deep within the magnetosphere, and, because of the large dipole tilt, they will have a profound and diurnally varying influence as absorbers of the trapped radiation belt particles.

AN INTRINSIC PLANETARY MAGNETIC field and magnetosphere at Uranus was discovered during the close approach by Voyager 2 on 24 January 1986. The instrumentation (*1*) for magnetic field measurements, which was used for the previous encounters with Jupiter and Saturn (*2*), operated normally throughout the encounter. The instrument automatically changes range as required by the measured field. The minimum quantization step size is ±0.002 nT in the lowest range (±8 nT full scale), increasing to ±0.51 nT in the ±2100-nT range used near closest approach. Vector measurements were obtained at a sampling rate of 16.67 Hz and were subsequently averaged over 1.92, 9.6, and 48 seconds, 8 and 16 minutes, and 1 hour for this study.

Because of the large inclination (97.8°) of the planet's equator to its orbital plane and that of Voyager 2's trajectory at encounter, the spacecraft covered a wide range of planetocentric latitude (from +59° to −78°) during the 45 hours that it was within the magnetosphere and magnetotail of the planet. There were no close encounters with any Uranian moon as by Voyager 1 at Titan (*3*).

Before the Voyager 2 encounter, the existence and characteristics of Uranus' magnetic field were uncertain because of the absence of nonthermal radio emissions (*4*). Observations since 1979 of hydrogen Lyman α emission by the International Ultraviolet Explorer were interpreted as being due to precipitating charged particles, which implied the presence of an active magnetosphere (*5*); there was no consensus on this interpretation, however (*6*). Our data and analysis have clarified a wide range of conjectures concerning the characteristics of the magnetic field and magnetosphere of Uranus (*7–12*).

The magnetopause and bow shock boundaries: Models and overview. Figure 1 shows the magnitude of the magnetic field and the associated pythagorean root-mean-square (RMS) deviation for 7 days around encounter. Bow shock and magnetopause crossings are indicated; times and corresponding distances are given in Table 1. These boundaries were identified with initial and, at times, incomplete data and are not final. The boundary crossings were used jointly to determine approximations to the global boundaries (Fig. 2).

The most unexpected and exciting result from this investigation is that Uranus' magnetic dipole is tilted far (60°) from the rotation axis; thus the magnetopause and bow shock contours vary with time as the planet and its field rotate, even for a constant external solar wind pressure. Two sets of various possible boundary profiles are shown in Fig. 2. At the time of the inbound magnetopause crossing, the spacecraft was at a magnetic colatitude (σ_m) of about 49°; therefore (ignoring second-order effects) the field pressure just within the magnetopause was then only 0.57 of its value at σ_m = 0° at the same distance from Uranus. This enabled the magnetopause near the spacecraft to assume the relatively closer position to the planet at that time. Because of this azimuthal asymmetry (about the x_0 axis in Fig. 2) of the internal field pressure, a smooth bulge occurs on the magnetopause near its intersection with an extension of the dipole axis; this position rotates with the planet. The bulge is estimated to be about a 10% to 15% effect. After encounter, the solar wind proton density and speed changed only slightly from their values before encounter (*13*). Therefore, the ratio of subsolar magnetopause distances before and after encounter, which presumably scales inversely as the 1/6-power law of momentum flux [as at Earth (*14*)], was treated as constant.

On the basis of our knowledge of Earth's magnetopause shape (*15, 16*), the lower

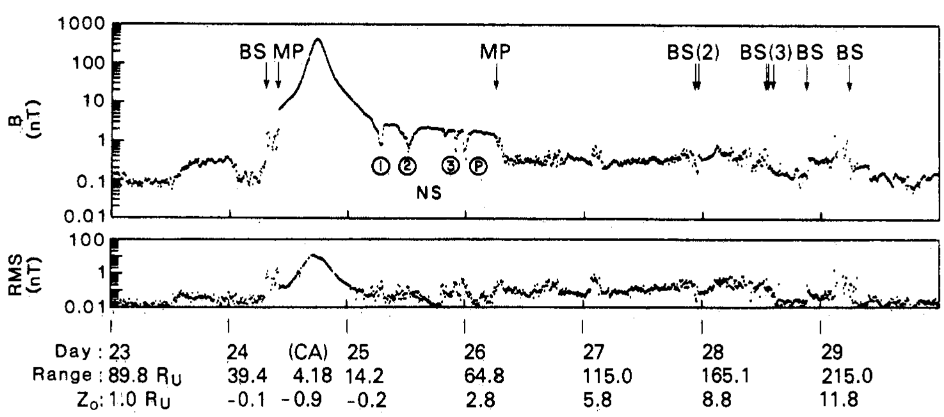

Fig. 1. The intensity of the magnetic field (B) and the pythagorean mean of the vector component root-mean-square (RMS) deviations, based on 8-minute averages. Abbreviations for crossings: BS, bow shock; MP, magnetopause; NS, neutral sheet; P, partial. The circled numerals indicate the three neutral sheet crossings. (Bottom) Planetocentric radial distance and Z_0 distance (see legend to Fig. 2) of the spacecraft. The large RMS values, which correlate with B near closest approach (CA), are an artifact due to spatial gradients in the field during the relatively long averaging interval used.

N. F. Ness, M. H. Acuña, K. W. Behannon, L. F. Burlaga, J. E. P. Connerney, R. P. Lepping, Laboratory for Extraterrestrial Physics, NASA Goddard Space Flight Center, Greenbelt, MD 20771.
F. M. Neubauer, Institut für Geophysik und Meteorologie, Universität Zu Köln, D-5000 Köln 41, Federal Republic of Germany.

Table 1. Bow shock (BS) and magnetopause (MP) boundaries and neutral sheet (NS) crossings.

Boundary	Center Time (day/hours: minute:second)	Planetocentric distance (R_U)*
BS	24/07:25:00	23.7
MP†	24/09:47:25	18.7
MP	24/10:07:10	18.0
Closest approach	24/17:58:24	4.2
NS1	25/06:59	28.7
NS2	25/12:31	40.6
NS3	25/22:09	60.8
NS (partial)	26/00:00	64.7
MP	26/06:20→07:50‡	79.6
BS	27/22:41:10	162.3
BS	27/23:01:05	163.0
BS	28/12:56:20	192.0
BS	28/13:02:15	192.2
BS	28/14:08→14:40	195
BS	28/21:25:50	209.6
BS	29/06:06:25	227.7

*1 R_U = 25,600 km. †Partial crossings between 24/09:47:25 and 24/10:07:10. ‡Time uncertain because of data gaps.

magnetopause was modeled with an ellipse and the upper magnetopause with a circle near the planet, smoothly connected at a point on the near tail boundary by a straight line of shallow slope (representing the tail boundary). The slope (tan 1.9°) of that line was chosen to equal that of the observed tail field just within the magnetopause. The derived normal to the inbound magnetopause surface was used as a constraint on the lower curve. The lower bow shock of Fig. 2 was also modeled by an ellipse and the upper bow shock with a circle close to the nose, matched to a straight line (representing the cross section of a shock Mach cone). The slope (tan 3.4°) was chosen to be that expected for the cold, fast solar wind at 19 astronomical units impinging on a blunt obstacle. The magnetosonic Mach number was estimated to be about 17. The two sets of bow shock and magnetopause curves were modeled such that they coincided at the subsolar point. Aberration due to planetary motion is small (<1°). The resulting subsolar magnetopause and bow shock distances are 17.8 and 22.5 Uranus radii (R_U), respectively. In the $x_0 = 0$ plane, which is nearly coplanar with that in which the planet's moons orbit, the magnetopause extended to between 25 and 33 R_U during encounter. Since Oberon's orbital radius is 22.9 R_U, all the known moons have orbits that are usually within the magnetosphere in this phase of the Uranian year and, to a slightly lesser extent, throughout its year.

Planetary magnetic field and rotation rate. Upon Voyager 2's entry into the Uranian magnetosphere, the observed magnetic field magnitude was approximately 7 nT (Fig. 1). The observed field magnitude then increased steadily to a maximum of 413 nT at 1756 spacecraft event time on day 24, just 2 minutes before closest approach (at 4.19 R_U). The field intensity then steadily decreased to 8 nT by 0200 on day 25. Within 12 R_U of the planet, the subspacecraft longitude varied by a full 360° cycle as the latitude changed from +52° to −78°. These wide ranges were particularly advantageous for the analysis and characterization of the planet's internal magnetic field.

Initial analyses established that the magnetic dipole axis was tilted by a large angle with respect to the rotation axis. These results were obtained by a spherical harmonic analysis (I1E1) to first order in internal terms (centered internal dipole) and to first order in external terms (uniform external field). However, in fitting 10-minute segments of data, a systematic drift (with time) of the dipole axis longitude was obtained. This implied that the rotation rate of the observed magnetic field was about 2° per hour less than that (23.12° per hour) adopted by the Voyager project well before encounter. Spherical harmonic analyses to second order in internal field (dipole plus quadrupole) and first order in external field (I2E1) resulted in a significantly better fit to the observations (0.92 nT RMS for distance less than 12 R_U) and a minimum in the RMS residuals corresponding to a rotation period of 17.29 ± 0.1 hours compared to the period of 15.57 hours selected before encounter. The magnitude of the quadrupole field in our initial analyses is substantial, and its contribution to the surface field of Uranus may be comparable to, or even larger than, that of the dipole. There is also evidence in the magnetic field observations of higher order (octupole) contributions.

For an initial model of the Uranian magnetic field, we adopted an offset, tilted dipole (OTD) representation. This model is particularly well suited for initial studies of charged particle motions in the magnetosphere. The best fitting OTD model has been derived by varying the location of the magnetic dipole to obtain a minimum RMS residual while also allowing the orientation and magnitude of the dipole to vary. The OTD model so obtained has a moment of 0.23 GR_U^3 and the positive pole tilted 60° from the rotation axis toward 48°W longitude, where longitude increases with time as seen from an inertially fixed point; this magnetic moment is close to one estimated by Van Allen (*17*) based on comparative planetology. The longitude of the spacecraft at 1800 of day 24 in this planet-centered coordinate system was 302°W. The OTD is located at $\Delta x = -0.02$ R_U, $\Delta y = +0.02$ R_U, and $\Delta z = -0.31$ R_U, with positive z in the direction of the planetary angular momentum vector. This OTD model fits the magnetic field observations within 12 R_U, with an RMS residual of 2.4 nT (Fig. 3).

A diagram of the magnetic field configuration is shown in Fig. 4. The magnetic field intensity on the planet's surface ranges from a low of about 0.1 G on the sunlit hemisphere to a maximum of about 1.1 G on the dark hemisphere. This 10:1 difference in surface field magnitude is far greater than that of either Jupiter or Saturn (*18*) and should lead to significant hemispherical differences in the altitude profiles of trapped and precipitating radiation belt particles. As shown in Fig. 4, the positive pole intersects the surface at +15.2°, 47.7°W and the negative pole at −44.2°, 227.5°W.

The magnetotail. The magnetosphere of

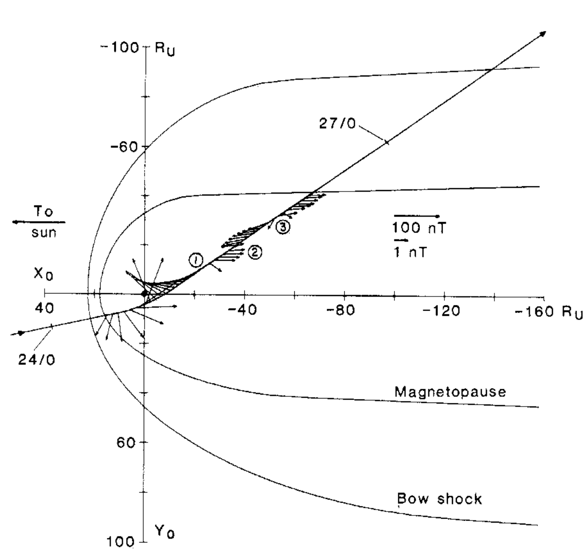

Fig. 2. Voyager 2's trajectory through the Uranian magnetosphere and representations of the planetary bow shock and magnetopause boundaries. The plane of projection is the Uranian orbital plane (x_0-y_0), where $+\hat{x}_0$ is sunward and $\hat{z}_0 = \hat{x}_0 \times \hat{y}_0$. The lower boundary curves are based on the observed inbound crossing locations, and the upper curves represent boundary shapes expected in the region $y_0 < 0$ about 5.5 hours later, when the planetary magnetic dipole (then near the x_0-y_0 plane) exerts increased internal field pressure on the $y_0 < 0$ portion of the magnetopause. The vectors along the trajectory are hourly averaged components of the magnetospheric field, scaled logarithmically. The circled numbers represent the three sequential transversals of the bipolar magnetic tail neutral sheet.

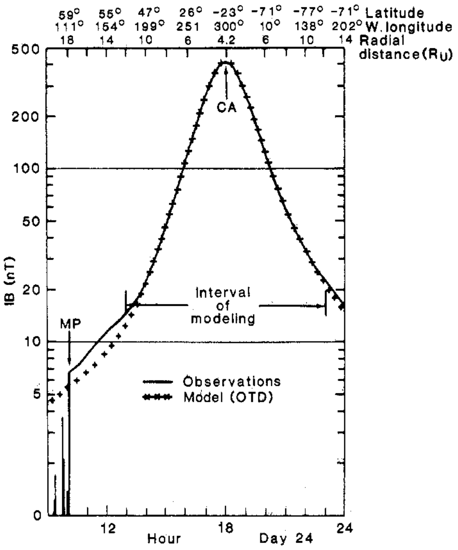

Fig. 3. Comparison of observed and modeled magnetic field intensity near encounter (from magnetosphere entry to exit). The RMS residual for this least-squares fit between 1300 and 2300 spacecraft event time (range < 12 R_U) is 2.4 nT.

Uranus has a fully developed magnetotail that is similar to Earth's in many of its characteristics. Voyager 2 was in the nightside magnetosphere tail region for 31 hours. The observed magnetic field direction was consistent with a progressive sweeping back of the planetary magnetic field by the solar wind to form a two-lobed, bipolar magnetic tail (Fig. 2). After Voyager 2's closest approach, the tail field rapidly approached an alignment either parallel or antiparallel to the planet-sun line out to the first magnetopause crossing at a radial distance of 79 R_U ($x_0 = -67\,R_U$). The estimated radius of the magnetic tail at that time was 42 R_U. Figure 2 indicates, with circled numerals, three complete crossings of the magnetotail field reversal region (plasma current sheet) separating the two lobes. The associated decreases in magnitude at the sheet crossings are illustrated in Fig. 1 and the crossing times are given in Table 1. Our initial analysis supports the conclusion that, within the region observed by Voyager 2, the tail rotates with the dipole motion but with slight (≈5.5°) helical twisting, significantly less than that proposed (*8, 10, 11*). Voyager 2 observed tail lobes of both polarities and the current sheet on both sides of the tail resulting from this rotation.

Figure 5 presents a view looking toward Uranus of the trajectory in the tail in the *y-z* plane in solar magnetosphere (SM) coordinates. The SM coordinates are right-handed; $\hat{x}_{SM}$ is toward the sun, and the plane x_{SM}-z_{SM} rotates to contain the dipole axis. The dashed curve through the sheet crossings is a possible sheet geometry. Through statistical analysis, Fairfield (*19*) found that the shape of Earth's neutral sheet is well represented by an ellipse. With only three crossings observed at Uranus, a rigorous curve fitting is not justified. The crossings are consistent with the parabola $y_{SM} = \pm 12(9 - z_{SM})^{1/2}$, giving an origin offset by 9 R_U along the $+z_{SM}$ axis. Taking this as the height of the hinge point of the current sheet gives an estimated hinge point distance of about 18 R_U along the extended magnetic equator in the midnight meridian plane. This is equal to the distance to the dayside magnetopause boundary found by Voyager 2. A similar equality has been found at Earth, where the stagnation point magnetopause distance and hinge point distance are both approximately 11 Earth radii on average (*15, 19*). The size of the diamagnetic decreases in field magnitude that occur at the neutral sheet crossings can be used to estimate the plasma sheet thickness; the initial estimate at the center of the tail is 10 R_U, increasing toward the flanks of the tail. This is approximately 25% of the tail radius and agrees well with the structure observed at Earth (*20*).

Initial analysis of the variation in magnetic field magnitude with increasing distance from Uranus in the tail indicates that, to a radial distance of about 25 R_U (up to the first current sheet traversal), the field decreased as a dipole. A markedly different gradient was observed beyond 25 R_U, with intensity decreasing with distance x_{SM} along the planet-sun line as $x_{SM}^{-0.6}$, compared with values at Earth between $x_{SM}^{-0.3}$ to $x_{SM}^{-0.7}$ (*21*). No clear difference in field strength between the two lobes was apparent in this study.

Interactions of the moons in the Uranian magnetosphere. The size of the Uranian magnetosphere (18 R_U sunward) observed by Voyager indicates that even the outermost moon Oberon (at 22.9 R_U) will spend a large fraction of its orbit inside the magnetosphere. The large tilt of the magnetic dipole axis leads to a dynamic situation in which the moons traverse a wide range of magnetic latitudes and longitudes. In so doing, the moons can effectively sweep up the trapped energetic charged particles from the magnetosphere (*22*). The relative positions of Voyager 2 and the moons can appropriately be described in terms of a well-known radiation belt coordinate system called (B, L) (*23*). The parameter L (in units of planetary radii) measures the magnetic equatorial distance to a field line about which energetic charged particles gyrate, and B is the minimum magnetic field intensity along a specific field line. In the degeneratively simple case of a dipole, we choose the origin to coincide with the location of the OTD and L to specify the positions of Voyager 2 and the moons.

Figure 6 illustrates the paths in L space followed by Voyager 2, Miranda, Ariel, Umbriel, and Titania as functions of spacecraft event time. The moons sweep through the magnetosphere in a complex way and can absorb (*22*) radiation belt particles with the same L, creating a dynamic magnetospheric structure. Particle absorption signatures are usually associated with the boundaries of the L space swept out by a particular moon. However, we emphasize the antici-

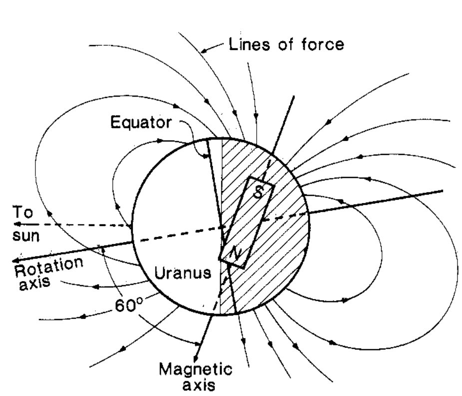

Fig. 4. Diagram of the OTD field lines in the meridian plane containing the OTD axis and rotation axis, illustrating the effects of the large angular (and spatial) offset from the rotation axis (and center) of Uranus.

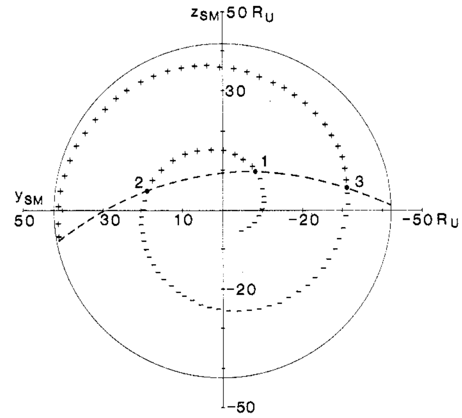

Fig. 5. The outbound Voyager 2 trajectory projected onto the solar magnetosphere *y-z* plane with a polarity indication of the lobe in which the spacecraft was located (+ field was away from the planet). Since z_{SM} rotates with the Uranian magnetic dipole, the spacecraft appears to trace out a spiral. Complete current sheet crossings are numbered as in Fig. 1. A model neutral sheet shape in cross section is given by the dashed curve. For reference, a circle is drawn with radius equal to the magnetopause crossing distance, assuming that the x_{SM} axis is coincident with the tail axis. Conservation of magnetic flux requires the actual tail axis to be displaced in the $+z_{SM}$ direction. The apparent angular displacement of the position of the symmetry axis of the estimated neutral sheet (dashed curve) from the z_{sm} axis is consistent with the slight helical twist found for the tail field lines (see text).

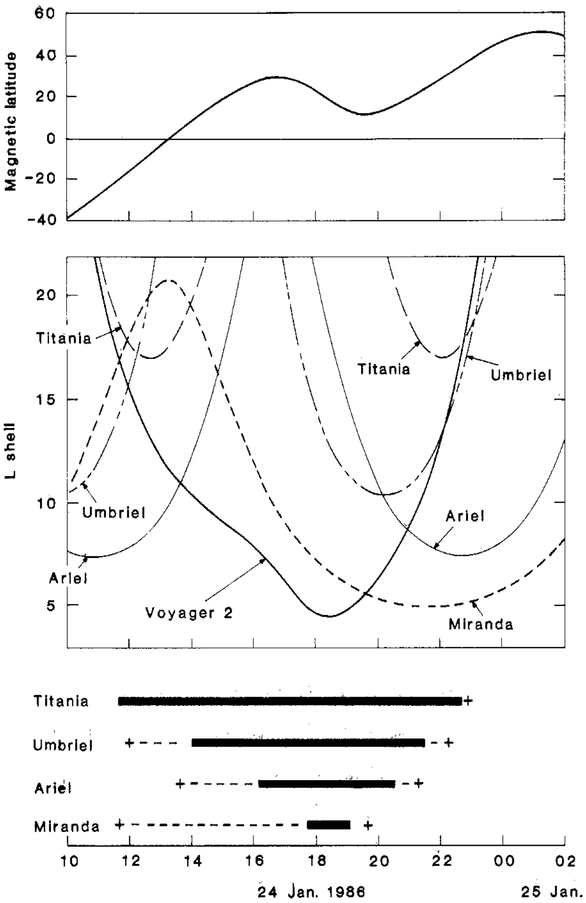

Fig. 6. Positions near encounter of Voyager 2 and the innermost four moons in terms of the magnetic L-shell parameter as functions of spacecraft event time. The spacecraft magnetic latitude is included at the top. The time intervals when Voyager was within the minimum L shell for each moon are indicated at the bottom as solid bars. The instantaneous L-shell intersections are denoted by (+).

pated need to consider the instantaneous L of both Voyager 2 and that moon because the drift periods of trapped particles can be short relative to the orbital periods of the moons. In fact, different energies and species of trapped particles have different drift periods, so that a proper interpretation of energetic particle observations requires detailed considerations. In Fig. 6 there is even an L-shell coupling between the moons as well as multiple candidates for absorption features. The predicted absorption regions based on the OTD model and indicated in Fig. 6 are in reasonable agreement with Voyager 2's radiation belt measurements (*24*).

The foot of the field lines threading Miranda and connecting it to Uranus' surface traces elliptical loci around the magnetic poles. The northern or sunlit ellipse extends approximately 65° in longitude and 32° in latitude, and the southern or darkside ellipse extends 55° in longitude and 20° in latitude. Footprint loci associated with more distant moons, as well as a possible "auroral zone," are proportionately smaller and fall within Miranda's footprint locus. The actual locations of these loci, especially those in the weak-field sunlit hemisphere, may be somewhat different because we used our simplified OTD model.

The interaction between a moon and the surrounding magnetospheric plasma depends on the properties of the moons and of the local magnetoplasma. If we assume rigid corotation, all flows past the Uranian moons are sub-Alfvénic because the plasma β, measuring the ratio of local energy density of particles to magnetic field energy density, is substantially less than 1 (*13*). No atmosphere has been observed around any of the moons, although a tenuous atmosphere due to sputtering and the accommodation of exospheric hydrogen can be expected (*25*); internal activity, such as volcanism, could also contribute to such an atmosphere. However, these atmospheres are not dense enough to produce an Io-type interaction (*26*). If the moons have no atmosphere and have high internal resistivity, the interactions will be superficially similar to the solar wind interaction with Earth's moon (*27*). Thus a shadow region should form, with small magnetic field perturbations and dimensions not much more than a moon diameter perpendicular to the magnetic field direction.

The moons and rings of Uranus are subjected to large, time-varying magnetic fields, particularly at and within the orbit of Miranda. It may be an important factor in the motions of very small particles in and between the rings if they are charged electrically. This could also be significant if the internal conductivity of the moon were high enough to permit electromagnetic induction to play an important role (*28*). The distortion of the ambient magnetic field near a moon with strong induction effects should have at least two consequences that are observable at large distances. Energetic particles with gyroradii much less than the moon's radius should experience reduced absorption. In addition, Alfvén waves will be launched along the field lines, eventually leading to coupling and energy transfer with the Uranian atmosphere-ionosphere system. The amount of induced current in the moon's interior may be sufficient to provide an important energy source through resistive (Joule) heating. This "AC" heating effect is different from the "DC" heating, such as at Io (*26*), that is due to the corotating magnetospheric field. At Miranda, the AC induction process may be much more important than the DC process.

Implications: The internal structure of Uranus. An active dynamo mechanism (*29*) rather than any permanent magnetization seems to be the most plausible way to explain the Uranian magnetic field. The question then immediately arises: At what radial range in the interior is a dynamo operating? Models of the interior of Uranus suggest a three-layer, spherically symmetric structure (*30*). The upper molecular layer consists mostly of hydrogen and includes the transition to the Uranian atmosphere. It is followed by an intermediate "oceanic" layer consisting of water and admixtures of other constituents. At the center is a "rocky" core containing mostly magnesium silicates and iron.

Several possibilities for the location of the Uranian dynamo region follow a priori from the requirement that an electrically conducting fluid must be present (*31*). The conductivity in the upper hydrogen layer must be too small to allow a dynamo. The first possibility is in the oceanic layer, where a lower limit for the conductivity may be 10^3 mho m^{-1} [the conductivity of high-pressure water (*32*)]. This value may be enhanced by the addition of constituents such as anions and cations leached out of the rocky core. Another possibility is in the lower parts of the "oceanic" layer, where a liquid, metallically conducting system with composition H-C-N-O and conductivity 10^5 mho m^{-1} may exist. A third possibility is the formation of a liquid iron inner core through differentiation of the rocky core, similar to Earth's, with 10^6 mho m^{-1} conductivity. A necessary condition for a dynamo to be active in any region is that there be sufficient energy available to balance the Joule dissipation in the dynamo region. A lower limit can be obtained from the Joule dissipation of the lowest order, free-decay mode in a sphere. In the "economic" Busse dynamo (*33*), a toroidal and a poloidal field of the same magnitude exist. Our estimates of the dynamo Joule dissipation suggest that the lower oceanic layer is slightly preferred because of a good compromise between a large radius and low resistivity.

We also can consider applying the scaling law for a Busse dynamo. Here we must note that other dynamo models generally address planetary fields with small tilts. For a Busse dynamo, the dipole moment is proportional to R^4, where R is the radius of the conducting dynamo region. With a rotation period of 17.3 hours for Uranus and calibration of the constant at Earth, we find that a dynamo in the lower "oceanic" part of Uranus is also most consistent with our results.

The possibility that we may be observing a polarity reversal, well known for the case of the terrestrial magnetic field (*34*) or the more general case of a nonsteady dynamo (*35*), cannot be ignored; the relatively large quadrupole components implied in our initial OTD field representation suggest that we consider this possibility. The observed large offset of the equivalent dipole is a question about which we can only speculate. Does it mean that the interior structure departs substantially from spherical symmetry? Or is it only the dynamo system that does? Is this due to a catastrophic collisional event subsequent to the formation of the planet, intimately related to its large and anomalous obliquity to the ecliptic? The continued study of these data may provide clues to the answer.

REFERENCES AND NOTES

1. K. W. Behannon *et al.*, *Space Sci. Rev.* **21**, 235 (1977).
2. N. F. Ness *et al.*, *Science* **206**, 966 (1979); N. F. Ness *et al.*, *ibid.* **215**, 558 (1982).
3. N. F. Ness, M. H. Acuña, K. W. Behannon, F. M. Neubauer, *J. Geophys. Res.* **87**, 1369 (1982).
4. M. L. Kaiser and M. D. Desch, personal communication; J. W. Warwick *et al.*, *Science* **233**, 102 (1986).
5. J. T. Clarke, *Astrophys. J.* **263**, L105 (1982); S. T. Durrance and H. W. Moos, *Nature (London)* **299**, 428 (1982); J. T. Clarke *et al.*, *Bull. Am. Astron. Soc.* **17**, 745 (1985).
6. R. V. Yelle and B. R. Sandel, *Geophys. Res. Lett.* **13**, 89 (1986).
7. G. L. Siscoe, *Planet. Space Sci.* **19**, 483 (1971); *Icarus* **24**, 311 (1975).
8. T. W. Hill, A. J. Dessler, M. E. Rassbach, *Planet. Space Sci.* **31**, 1187 (1983).
9. G.-H. Voigt, T. W. Hill, A. J. Dessler, *Astrophys. J.* **266**, 390 (1983).
10. T. W. Hill, in *Uranus and Neptune*, J. T. Bergstrahl, Ed. (*NASA Conf. Publ. 2330*, 1984), p. 497.
11. ——— and A. J. Dessler, *Science* **227**, 1466 (1985).
12. S. A. Curtis and N. F. Ness, *Geophys. Res. Lett.* **12**, 855 (1985).
13. H. S. Bridge *et al.*, *Science* **233**, 89 (1986).
14. J. T. Choe, D. B. Beard, E. C. Sullivan, *Planet. Space Sci.* **21**, 485 (1973).
15. D. H. Fairfield, *J. Geophys. Res.* **76**, 6700 (1971).
16. J. A. Slavin, R. E. Holzer, J. R. Spreiter, S. S. Stahara, D. S. Chanssee, *ibid.* **88**, 19 (1983).
17. J. A. Van Allen, in *Highlights of Astronomy*, E. A. Müller, Ed. (International Astronomical Union, Paris, 1977), vol. 4, part 1, pp. 195–224.
18. M. H. Acuña and N. F. Ness, *J. Geophys. Res.* **81**, 2917 (1976); E. J. Smith, L. Davis, Jr., D. E. Jones, in *Jupiter*, T. Gehrels, Ed. (Univ. of Arizona Press, Tucson, 1976), p. 788; E. J. Smith *et al.*, *J. Geophys. Res.* **85**, 5655 (1980); J. E. P. Connerney, N. F. Ness, M. H. Acuña, *ibid.* **88**, 8771 (1983).
19. D. H. Fairfield, *J. Geophys. Res.* **85**, 775 (1980).
20. S. J. Bame, J. R. Asbridge, H. E. Felthauser, E. W. Hones, I. B. Strong, *ibid.* **72**, 113 (1967).
21. K. W. Behannon, *ibid.* **73**, 907 (1968); J. D. Mihalov, D. S. Colburn, R. G. Currie, C. P. Sonett, *ibid.*, p. 943; J. A. Slavin, B. T. Tsurutani, E. J. Smith, D. E. Jones, D. G. Sibeck, *Geophys. Res. Lett.* **10**, 973 (1983).
22. G. D. Mead and W. N. Hess, *J. Geophys. Res.* **78**, 2793 (1973).
23. C. E. McIlwain, *ibid.* **66**, 3681 (1961).
24. E. C. Stone *et al.*, *Science* **233**, 93 (1986); S. M. Krimigis, *ibid.*, p. 97.
25. A. F. Cheng, in *Uranus and Neptune*, J. T. Bergstrahl, Ed. (*NASA Conf. Publ. 2330*, 1984), p. 541.
26. F. M. Neubauer, *J. Geophys. Res.* **85**, 1171 (1980).
27. N. F. Ness, in *Solar Terrestrial Physics/1970*, E. R. Dyer, Ed. (Reidel, Dordrecht, Netherlands, 1972), part 2, pp. 159–205.
28. G. Schubert and K. Schwartz, *Moon* **1**, 106 (1969); C. P. Sonett, B. F. Smith, D. S. Colburn, G. Schubert, K. Schwartz, *Proc. Lunar Sci. Conf.* **3**, 2309 (1972).
29. M. Torbett and R. Smoluchowski, *Nature (London)* **286**, 237 (1980).
30. W. B. Hubbard, in *Uranus and Neptune*, J. T. Bergstrahl, Ed. (*NASA Conf. Publ. 2330*, 1984), p. 291.
31. E. N. Parker, *Astrophys. J.* **122**, 293 (1955).
32. A. C. Mitchell and W. J. Nellis, *J. Chem. Phys.* **76**, 6273 (1982).
33. F. H. Busse, *Phys. Earth Planet. Int.* **12**, 350 (1976).
34. M. D. Fuller, J. W. Williams, K. I. Hoffman, *Rev. Geophys. Space Phys.* **17**, 179 (1979).
35. D. J. Stevenson, *Rep. Prog. Phys.* **46**, 555 (1983).

36. We thank our colleagues at Goddard, those involved with the Voyager CRS, LECP, PLS, and PRA investigations, and S. A. Curtis, D. J. Stevenson, and J. A. Van Allen for discussions of these results. We also thank the entire Voyager project staff at the Jet Propulsion Laboratory, especially G. Sisk, E. Franzgrote, N. Toy, H. Woo, O. Divers, and W. McDougal, for the success of the mission and their support of our investigation; W. Mish and his data processing and analysis team, particularly T. Vollmer, P. Harrison, J. Jones, T. Carleton, J. Annen, G. Burgess, J. Byrnes, S. Kempler, L. Moriarty, F. Ottens, A. Silver, and R. Thompson, for support; C. Moyer, J. Scheifele, J. Seek, and E. Worley for contributions to the design, development, and testing of the hardware; and F. Hunsaker and L. White for technical assistance. F.M.N. was supported financially by the German Ministry of Science and Technology.

2 April 1986; accepted 5 May 1986

Plasma Observations Near Uranus: Initial Results from Voyager 2

H. S. Bridge, J. W. Belcher, B. Coppi, A. J. Lazarus, R. L. McNutt, Jr., S. Olbert, J. D. Richardson, M. R. Sands, R. S. Selesnick, J. D. Sullivan, R. E. Hartle, K. W. Ogilvie, E. C. Sittler, Jr., F. Bagenal, R. S. Wolff, V. M. Vasyliunas, G. L. Siscoe, C. K. Goertz, A. Eviatar

Extensive measurements of low-energy positive ions and electrons in the vicinity of Uranus have revealed a fully developed magnetosphere. The magnetospheric plasma has a warm component with a temperature of 4 to 50 electron volts and a peak density of roughly 2 protons per cubic centimeter, and a hot component, with a temperature of a few kiloelectron volts and a peak density of roughly 0.1 proton per cubic centimeter. The warm component is observed both inside and outside of $L = 5$, whereas the hot component is excluded from the region inside of that L shell. Possible sources of the plasma in the magnetosphere are the extended hydrogen corona, the solar wind, and the ionosphere. The Uranian moons do not appear to be a significant plasma source. The boundary of the hot plasma component at $L = 5$ may be associated either with Miranda or with the inner limit of a deeply penetrating, solar wind–driven magnetospheric convection system. The Voyager 2 spacecraft repeatedly encountered the plasma sheet in the magnetotail at locations that are consistent with a geometric model for the plasma sheet similar to that at Earth.

Before the Voyager 2 flyby, nothing was known about the plasma environment of Uranus or about the interaction between the planet and the solar wind. Various speculative models had been proposed (*1–6*) that were based on differing assumptions about plasma processes and on estimates of the planetary magnetic field that ranged from 0 G to more than 10 G. We now describe Voyager 2's observations of the spatial distribution and physical properties of the plasma near Uranus.

The Voyager plasma science (PLS) experiment (*7*) detects positive ions and electrons with energies-per-charge from 10 V to 6 kV. Figure 1 shows an overview of ion and electron fluxes measured near Uranus along the spacecraft trajectory, which is il-

H. S. Bridge, J. W. Belcher, B. Coppi, A. J. Lazarus, R. L. McNutt, Jr., S. Olbert, J. D. Richardson, M. R. Sands, R. S. Selesnick, J. D. Sullivan, Center for Space Research, Massachusetts Institute of Technology, Cambridge, MA 02139.
R. E. Hartle, K. W. Ogilvie, E. C. Sittler, Jr., NASA–Goddard Space Flight Center, Greenbelt, MD 20771.
F. Bagenal, Imperial College, London, England.
R. S. Wolff, Jet Propulsion Laboratory, California Institute of Technology, Pasadena, CA 91109.
V. M. Vasyliunas, Max-Planck-Institüt für Aeronomie, Katlenburg-Lindau, Federal Republic of Germany.
G. L. Siscoe, Department of Atmospheric Science, University of California, Los Angeles, CA 90024.
C. K. Goertz, Department of Physics and Astronomy, University of Iowa, Iowa City, IA 52242.
A. Eviatar, Department of Geophysics and Planetary Sciences, Tel Aviv University, Tel Aviv, Israel.